Radial Glial from mammalian developing neocortex can divide symmetrically in vitro

Mario Ledesma-Terrón, Nuria Peralta-Cañadas, David G. Míguez*

Departamento de Física de la Materia Condensada
Centro de Biología Molecular Severo Ochoa, CBMSO
Instituto de Física de la Materia Condensada, IFIMAC
Instituto Nicolás Cabrera, INC
Universidad Autónoma de Madrid, 28012, Spain
Corresponding author: david.miguez@uam.es

Abstract

Radial Glial progenitors in the mammalian developing neocortex follow a deterministic differentiation program restricted to an asymmetric only mode of division. This contrast with many other developmental systems, such as the developing spinal cord, the retina, epidermis, airway epithelium, germline, and the intestine, where the fate at the single cell level is unpredictable, and differentiation takes place based on probabilities that can change overtime. Here, we combine experimental, computational and theoretical tools to show that Radial Glial cultured *in vitro* also divide symmetrically, and that the balance between different modes of division can be modulated by external signals, such as Fibroblast Growth Factor. Our results suggest that the constraint of deterministic and asymmetric mode of division of Radial Glial is not an inherent property of this particular cell type, but a feature induced by the complex organized pseudo-stratified structure of the mammalian developing neocortex.

Keywords: cell cycle, differentiation, Branching Processes

1. Introduction

The neocortex constitutes the main part of the mammalian brain, and the location where the processing of all higher-order brain functions resides. Understanding its formation is one of the major interests of Developmental Biology [1]. The neocortex develops from a stratified neuroepithelium called the neural tube into a complex structure of six horizontal layers of excitatory and inhibitory neurons [2]. Neurogenesis in the developing neocortex initiates when neuroepithelial progenitors transform into Radial Glial (RG) progenitor cells and start to produce neurons and intermediate neuronal precursors [3, 4]. Since the discovery that RG constitute the progenitors of potentially all neurons in the vertebrate neocortex [5, 6, 7, 8], a great effort has been focused in identifying their features and properties: how they coordinate in time and space to form the multiple layers of the neocortex?; which signals control their fate?; and how these signals orchestrate the correct balance between proliferation or differentiation during neurogenesis?.

In principle, this balance can be robustly achieved via stochastic or deterministic cell decisions [9]. In brief, stochastic models assume certain probability of differentiation that depends on the intracellular and extracellular signals that the cell is receiving. In this context, the fate at the single cell level is unpredictable and the balance between proliferation and differentiation is regulated at the level of the population [10].

On the other hand, deterministic models of stem cell differentiation assume that the fate of cell is an intrinsic property of the cell and the correct balance between numbers of different types of neurons is achieved at the level

of a single cell [11].

The dynamics of differentiation is often characterized based on the fate of the two daughter cells of a cell division relative to each other [12]. This way, proliferating progenitors can perform *pp* (progenitor-progenitor), *pd* (progenitor-differentiated) and *dd* (differentiated-differentiated) divisions [13].

In this context, differentiation in the developing chick spinal cord [14], in the zebrafish retina [15, 16], epidermis [17], airway epithelium [18], germline [19], and the intestine [20] of mice follow an stochastic model. In these systems, progenitors can potentially perform each of the three types of division, and the corresponding rates are probabilistic and change overtime.

On the other hand, the formation of neurons in the mammalian brain has been shown to follow a deterministic mode: neuroephitelial progenitors can divide only symmetrically (*pp*), while RG only divide asymmetrically (*pd*) [21, 3]. In this direction, it has been shown using clonal analysis that neurogenesis in mouse occurs in a well ordered and deterministic manner, where each RG produces around 8-9 neurons via only an asymmetric mode of division [21, 3] with a cell cycle of (16-18 h).

This important difference between the deterministic mode of division in the developing neocortex compared to other neurogenic tissues suggested us to investigate whether the deterministic nature of RG is an intrinsic property of this particular cell type or if, on the other hand, it is a property provided externally. In this scenario, RG should be able to perform also *pp* and *dd* type of divisions when cultured *in vitro*.

To do that, we develop an experimental, computational and theoretical approach that combines *in vitro* cultures of RG from mouse developing

cerebral cortex with automated image segmentation, processing and quantification algorithms. Quantitative values of cell numbers are then used to inform a theoretical framework based on a branching process formalism [14]. Our results shown that RG are able to divide both symmetrically and asymmetrically when cultured *in vitro*, and that the average mode of division changes overtime, as well as the average cell cycle length [14]. In addition, the mode of division can be modulated by external cellular signals, such as Fibroblast Growth Factor (FGF). Our results suggest that the deterministic mode of differentiation or RG is not an intrinsic property of the cells, and therefore, it may be imposed by the spatio-temporal restrictions provided by the stratified organization of the developing neocortex.

2. Results

2.1. RG proliferate in culture at a rate dependent on FGF stimulation

To initially test if the dynamics of RG growth and differentiation *in vitro* recapitulate *in vivo* observations, RG from mouse embryo developing neocortex are extracted, plated and cultured following standard protocols [22]. Starting at 24 hours post extraction (hpe) from mice embryos to allow cells to recover and attach to the substrate, samples are then fixed at three different time points and stained with Hoechst (Fig. 1A). Quantification of the number of cells in a field of view of fixed size using an automated segmentation tool (see Methods) is shown in Fig. 1B for two culture conditions: control and +FGF, where the standard culture media is supplemented with an increased concentration of FGF ligand (see Methods).

In both conditions, the size of the population seems to grow, but only

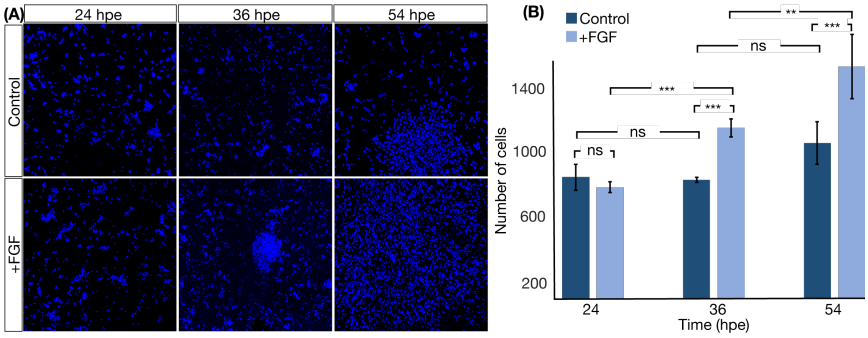

Figure 1: **The growth rate of the population of RG can be modulated by FGF stimulation.** (A) Snapshots of RG cultures at different hours post extraction (hpe) stained with Hoechst and growing at control and +FGF culture conditions. (B) Quantification of total cell numbers in an area of the culture of fixed dimensions at different time points shows that cells under extra FGF stimulation show increased proliferation with statistical significance. *** = $p < 0.005$, ** = $p < 0.05$, ns = not statistically significant. Error bars correspond to standard error of the mean value between multiple samples of similar conditions.

growth of the culture in +FGF conditions is statistically significant, compared to control and to the other time points of the same condition. This results suggest that the proliferation dynamics of RG can be modulated when cultured *in vitro*.

2.2. FGF stimulation of RG cultures result in shorter cell cycle length

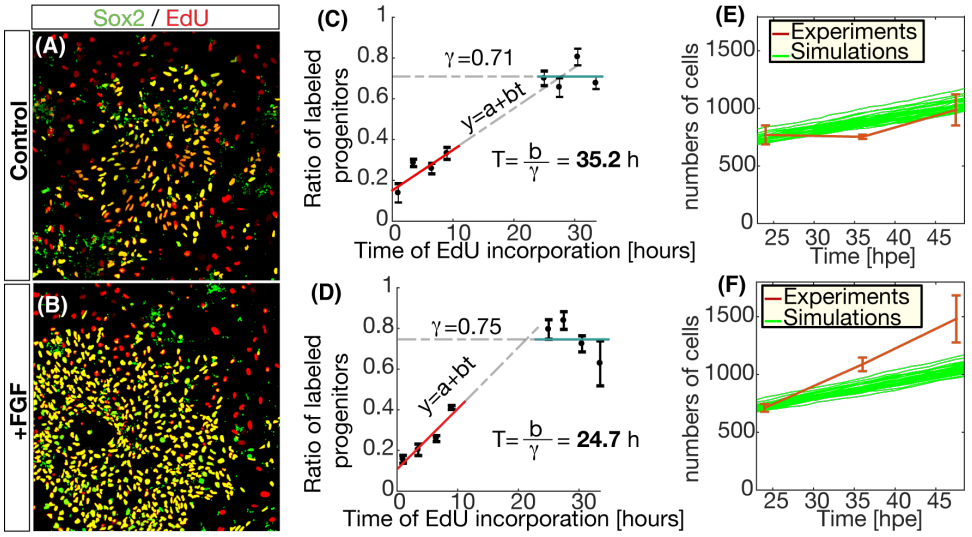

Figure 2: **Increased FGF result in a shortening of the division time of cycling RG.** (A-B) Snapshots of *in vitro* cultures stained with Sox2 (green) to label RG and EdU (red) to label cells that have undergo S-Phase. Snapshots correspond to 24 hours of Edu incubation. (C-D) Cumulative curve quantification of EdU positive progenitors in the culture versus EdU incubation time. Cells under extra FGF cycle faster (T= 24.7 hours) than control cells (T=35.2 hours). The growth fraction γ is similar for both conditions. (E-F) Numerical simulations of an model of cycling and differentiating RG (green lines) show that the experiments (red data points) fits with a scenario with constant cell cycle and restricted asymmetric division of the RG for control condition, but not for +FGF conditions.

In principle, increased growth rate in a differentiating stem cell population

can be caused by changes in the number of cycling cells, reduced cell death, reduced differentiation rate or a direct effect in the cell cycle dynamics. To study how FGF affects the dynamics of growth of a culture of RG, we perform 5-ethynyl-2'-deoxyuridine (EdU) cumulative labeling experiments. To do that, samples are cultured in he presence of Edu and then fixed at different time points (corresponding to different EdU incubation times). Combined nuclear Hoechst staining with immunostaining against EdU and Sox2 is used to identify all neural progenitors cells that have passed through S-phase for each EdU incubation time.

Quantification using an automated image segmentation algorithm (details are explained in the Methods section) is used to calculate the cell cycle length and the growth fraction using linear regression (see Methods). Results are shown in Fig. 2. The data (Figs. 2C,D) reveals that the growth fraction γ remains at around 80% for both conditions tested. On the other hand, the cell cycle length of the population appears to be highly dependent on the culture conditions. Control cells cycle at a rate of T=35.2 hours, while cells under extra FGF stimulation show a faster division time (T=24.7 hours). Therefore, our results show that FGF stimulation shortens the cell cycle length in cultures of RG *in vitro*.

2.3. EdU estimation of cell cycle and asymmetric mode of division do not reproduce the experimental observations

Next, we ask whether the values of cell cycle length measured with EdU cumulative labeling can account for the dynamics of the population of RG observed in Fig 1B. To do that, we developed a computational model of a generic differentiating stem cell population that simulates cycling progenitors

that can either proliferate, differentiate, enter quiescence of apoptosis based on rates provided by the user. Details of the model are presented in the Methods section. A scheme of the simulation framework is shown in Supp Fig 1. Parameters can be kept constant throughout the simulation, or can be set to change each time-step. Parameter values are sampled from a gamma distribution to mimic variability.

The model is then informed with the values of initial number of cells, cell cycle and the growth fraction measured in the previous section (cell death is set to zero). Following the literature on RG proliferation and differentiation dynamics [21, 3], the division mode is restricted to deterministic and asymmetric *pd*. Results are shown in Fig. 2E,F for 30 independent numerical simulations (green lines). The dynamics of the control conditions closely resembles the experimental data (red), while in extra FGF conditions the simulation population grows at a rate much lower than the experimental culture.

In conclusion, the numerical model shows that the changes in cell cycle length alone are not sufficient to explain the increased growth rate observed in +FGF conditions, and therefore, other features are being affected by FGF.

2.4. FGF increases the production of progenitors as well as terminally differentiated neurons

To test if the changes in the culture conditions could also alter the balance between proliferative versus differentiated cells in the population we perform additional experiments where the RG are extracted and cultured under the conditions described in the Methods section. Starting at 24 hpe, samples are cultured and fixed every 2-4 hours and stained using antibodies against Sox2

and Map2 to identify progenitors and differentiated cells, respectively. We then automated the segmentation and quantification of each cell type using a computational script that identifies the fate of each cell in the population based on the intensity of Sox2 and Map2 staining (details are described in the Methods section).

Results are shown in Fig. 3 for the two conditions tested: control and +FGF. Output provided by the segmentation script is plotted in Figs 3B,C. The average dynamics of growth of the population is obtained by nonlinear sigmoidal fitting of the experimental values (green, red, and blue lines for RG, neurons and total cells, respectively). The data shows that an initial regime of reduced change in cell numbers is followed by an increase in both cell types until the system reaches a regime where few new cells are being generated. In both conditions, the amount of progenitors and differentiated cells increases as time progresses, with a higher increase of both cell types in conditions of +FGF stimulation.

In conclusion, the addition of FGF results in more progenitors and differentiated cells, and not an increased in one population to the expenses of the other (consistent with a reduced cell cycle length). On the other hand, the population of RG (green data points, green line), increases significantly in +FGF conditions. This is inconsistent with the observation that RG from mouse neocortex can only divide asymmetrically *in vivo* [21, 3] (in this scenario, the total amount of RG cells should remain constant or close to a constant value).

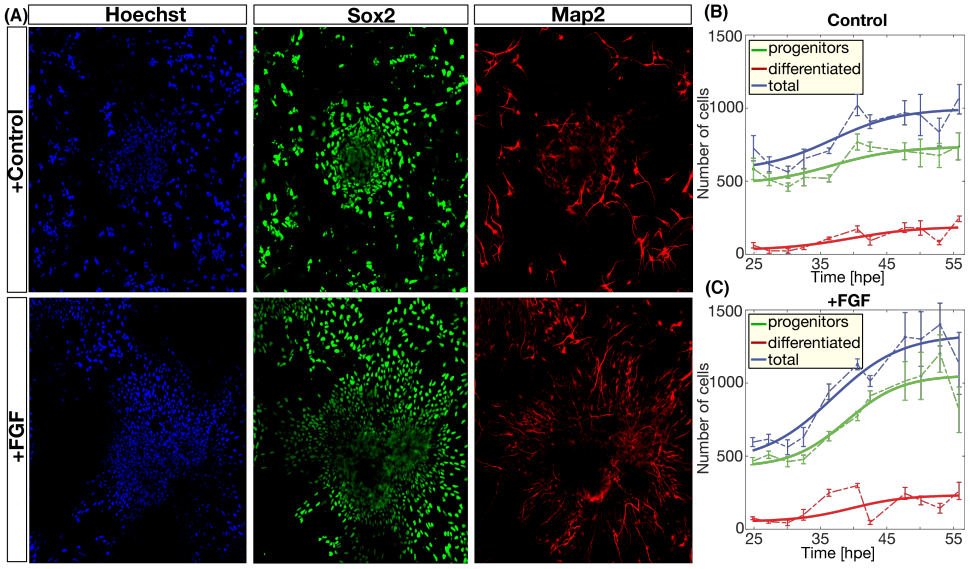

Figure 3: **FGF increases the amount of RG as well as terminally differentiated neurons.** (A) Snapshots of RG cultures at 24 hours post extraction showing nuclei (Hoechst), progenitors (stained with Sox2) and differentiated neurons (stained with Map2). (B-C) Quantification of the number of cells of each type in both culture conditions shows an increased number of progenitors and differentiated cells, compared to control conditions. Error bars correspond to standard error of the mean. Lines correspond to nonlinear sigmoidal fitting of the experimental data points.

2.5. Branching process formalism predicts variable mode and rate of division

The previous observation suggests that, apart from the changes in the cell cycle length, FGF is affecting also the mode of division of the RG. To study the dynamics of the mode of division during the experiment, we will take advantage of the theoretical framework developed by our lab and introduced in Ref [14]. In brief, the approach uses a branching process formalism to obtain analytical equations that provide the average values of proliferation and differentiation of the population based only on changes in the number of progenitors (P) and differentiated cells (D).

To do that, numbers of P and D provided by our automated quantification in previous sections are used as input of the following equations for the mode and rate of division, which correspond to a generalization of Equations presented in Ref. [14] that now accounts for a potential reduction of the progenitor pool:

$$pp - dd = \frac{1 + \emptyset_P(\frac{\Delta D}{\Delta P} - 1)}{\frac{\Delta D}{\Delta P} + 1} \quad (1)$$

$$T = \Delta t \frac{log(1 + \gamma|pp - dd - \emptyset_P|)}{\Psi log \frac{P_t}{P_0}} \quad (2)$$

where pp and dd correspond to the rate of symmetric proliferative and differentiative divisions, respectively. $\Delta P = P_t - P_0$ and $\Delta D = D_t - D_0$ correspond to the number of progenitors and differentiated cells generated in a given window of time $\Delta t = t - t_0$. The value $pp - dd$ goes from 1 (all divisions are symmetric proliferative) to -1 (all divisions are symmetric differentiative). The value, $pp - dd = 0$ corresponds to maintenance of the progenitor pool, either via asymmetric pd divisions of via balance between symmetric prolif-

erative and differentiative divisions (the model cannot distinguish between these two scenarios, since they are mathematically equivalent). Ψ takes the value of 1 when $1 \leqslant pp - dd < 0$, while for values between $0 \leqslant pp - dd \leqslant -1$ takes the form $\Psi = (0.9|pp - dd| - 1)$. $\emptyset_P$ is the rate of cell death of the progenitors pool. Assuming that most cell death occurs via apoptosis, the value of $\emptyset_P$ is obtained using double immuno-labeling against Sox2 and Cleaved Caspase3 (see Supp Fig 2 A-B).

Parameter γ corresponds the growth fraction, which are obtained using double immuno-labeling against Sox2 and Ki67 (see Supp Fig 2 C-D).

Output of the equations is shown in Fig. 4A for the average cell cycle length T. Our data shows that the cell cycle length is not constant throughout the experiment, showing initially very high cell cycling times, followed by a regime of faster proliferation and finally again a regime of reduced proliferation. Interestingly, the minimum of the cell cycle for both conditions tested occurs around 36-37 hours post extraction, with the value of control conditions around T= 19 hours and, T= 10 hours for +FGF conditions.

Fig 4B shows the prediction for the average mode of division *pp-dd*. In both cases differentiation appears to increase with time, and this change is more prominent in conditions of extra FGF.

Interestingly, both situations show values of $pp - dd$ different from the value of $pp - dd = 0$ (i.e., $pd = 1$), that could indicate a restricted asymmetric differentiating of RG. In addition, the maximum change in the differentiation dynamics occurs around 36-37 hpe, coinciding with the minimum of T of both conditions. In conclusion, quantification of the cell numbers using our branching process framework suggest that the presence of FGF in the culture

media speeds up the cell cycle time, reduces the differentiation rate and slightly increases the growth fraction (Supp Fig 2 C-D).

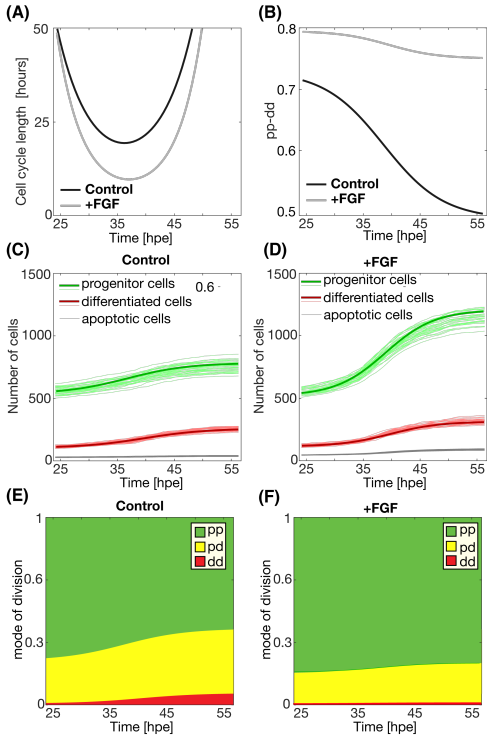

Figure 4: **FGF affects the proportion of symmetric proliferative divisions in RG culture** (A-B) Plot of the average T (A) and $pp - dd$ of the population of RG under control (black) and +FGF (grey) conditions. (C-D) Simulations (light red and green lines) for both conditions using parameters of mode and rate of division of (A-B). Thick lines correspond to the sigmoidal fitting of the experimental data in Fig. 3. (E-F) Prediction for each mode of division using a stochastic model of differentiation.

2.6. Values from the branching process analysis are able to reproduce the experimental data

To test if the values provided by the branching process formalism are correct, we take advantage of the same numerical model of the differentiating

stem cell population introduced previously. Now, the model is informed with the prediction of T and $pp - dd$ plotted in Fig. 4A-B. The growth fraction and apoptosis rate are also obtained from the experimental data in Supp Fig 2. Results are plotted in 4C-D, where we plot the number of progenitors and differentiated cells (thin green and red lines, respectively) for 30 independent simulations on top of the sigmoidal fitting of the experimental values of progenitors and differentiated cells (thick green and red lines, respectively). Simulations are in good agreement with the experimental data for both conditions, suggesting that the branching equations predicts the correct mode and rate of division.

2.7. The number of RG labelled after a short EdU pulse increases in time

To validate the outcome of the branching process formalism that predicts a non negligible number of *pp* divisions are taking place in the culture, we designed an experiment based on Pulse-and-Chase of EdU labelled cells. Do do that, we extracted cells from mouse developing neocortex following the procedure explained in Methods section. Next, cell are cultured in control and +FGF conditions until 33 hpe (when the cell cycle length is fastest, Fig. 4A). At this point, a pulse of 30-minutes of EdU is applied to all samples. A number of samples are fixed at this time (Pulse time point). After washing the EdU (see methods) from the culture media, cells are cultured for another 15 hours (corresponding to the predicted average cell cycle length for +FGF conditions during this time) to ensure that labeled cells cannot cycle more than once in any of the culture conditions. Next, cells are fixed and stained with Hoechst, EdU and Sox2 immunostaining. Finally, the number of Sox2+/EdU+ cells at the time of the pulse (33 hpe) and chase (47 hpe) is

quantified using our automated image analysis tool (see Methods). Results are shown in Fig. 5. The number of progenitors labeled with EdU does not change significantly in control conditions, consistent with a large proportion of asymmetric divisions (i.e, one EdU+ RG produces two EdU+ cells: one RG and one neuron, so the amount of EdU+ RG remains constant). On the other hand, in conditions of +FGF, we see a statistically significant increase in the number of EdU+ RG when comparing pulse and chase time points. This result shows that some of the RG originally labeled with the short EdU pulse, divided and produced more than one RG per division, showing that, as predicted by the branching formalism, RG are capable to undergo pp divisions *in vitro*.

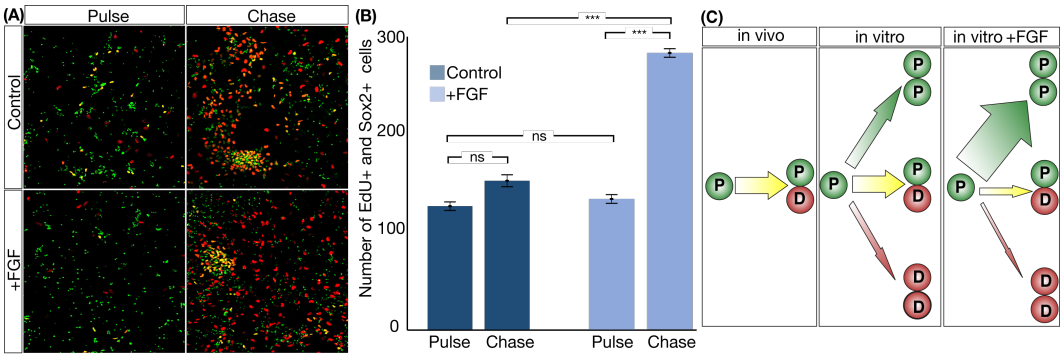

Figure 5: **Pulse-Chase experiments shows increased EdU labeled RG cells in presence of an extra concentration of FGF**. (A) Representative images showing Sox2 and EdU staining in green and red, respectively. (B) Quantification of the number of Sox2 and EdU positive cells for Pulse and Chase time-points for control and FGF+ conditions. The number of EdU labelled RG cells increases in the Chase time-point in conditions of +FGF with statistical significance. *** = $p < 0.005$, ns = not statistically significant. Error bars correspond to standard error of the mean value between multiple samples of similar conditions. (C) Scheme that summarizes the experimental observations.

2.8. The Branching equations outperform EdU cumulative methods to measure cell cycle length

BrdU [23], EdU [24, 25] and other thymidine analogs constitute the most used tool to estimate the cell cycle length of cells in many contexts [26]. The methodology is based on the replacement of endogenous thymidine during DNA synthesise with traceable compounds [27, 28]. The length of the average cell cycle is then inferred from the dynamics of the incorporation of these compounds into the DNA of cycling cells [29].

The use of thymidine analogs has several drawbacks: it can be toxic and mutagenic [30] and affect the normal dynamics of cell proliferation [31] by lengthening the cell cycle. In addition, choosing the correct mathematical analysis and interpretation of the experimental data is not straightforward [32]. Authors have proposed several approaches, such as linear [33, 34], non-linear fitting [35, 36], or the use of deterministic [37] or stochastic models [38]. Depending on the method used, the same input data results in quite different predictions for the average duration of the cell cycle [39]. Due to these limitations, BrdU and analogs have been referred as "one of the most misused techniques in neuroscience" [40].

To try to understand the discrepancy between the cell cycle length measured using EdU cumulative curve (Fig 2) and the branching process formalism (Fig 4), we take advantage of the numerical model presented previously. The model is now modified to simulate EdU labeling (cells in S-phase are marked as labeled when EdU is present). Then, the number of progenitors, differentiated and EdU positive progenitors at each time point is used to calculate the average cell cycle length of the population using three widely

used EdU based methods: single cumulative curve (SC) [23], dual cumulative (DC) using two thymidine analogs in combination [41], and the pulse-chase (PC) method [36] (see Methods and Supp Fig 3 for a detailed explanation of each protocol). The cell cycle is also calculated using the branching process (BP) method [14]. All predictions are then compared with the real value of T used for each simulation, to estimate the accuracy and reliability of each method.

The first scenario tested corresponds to homeostasis in the progenitor population ($pp - dd$=0), constant value of T=20 hours and no quiescent or apoptotic cells ($\gamma = 1, \emptyset_P = 0$). These are the conditions defined by Nowakowski and coworkers when introducing the cumulative curve method [23].

Results of the analysis are plotted in Fig. 6A. Dots in Fig. 6B correspond to the prediction of the value of T for 10 independent simulations (crosses represent the average). We see that, for these particular settings, all four methods are able to predict the correct value of T (dashed line) within a 10% error margin, with both PC and BP performing slightly better than SC and DC. Importantly, the values predicted by the 10 simulations for the two cumulative methods show a high dispersion. This suggests that large number of repeats should be necessary to get an accurate value of T (the typical experimental design that involves only three independent repeats does not guarantee a correct estimation of the cell cycle). The same conclusions apply when considering our experimental conditions of growth of the population of progenitors ($pp - dd > 0$, Supp. Fig. 4A).

Fig. 4A shows a decrease of cell cycle length followed by an increase.

Variable cell cycle dynamics has been reported in many developmental systems [42, 43, 14, 44, 45, 46, 47, 48, 49, 50, 42, 43, 51, 52]. Fig. 6C corresponds to output of the numerical model when a variable value of T is used as input. The average value of T was set to 20 hours. Fig. 6D plots the quantification of the numerical data. In this situation, SC predicts a much longer cell cycle that the average (49% error), while the DC predicts a shorter cell cycle (24% error). Interestingly both PC and BP return a value much closer to the correct average, with less than 10% error. Again, the variability of the cumulative methods is very high, making them unreliable methods when a small number of repeats are used. Again, the same conclusions apply when considering conditions where the cell cycle changes while the population of progenitors is allowed to grow ($pp - dd > 0$, Supp. Fig. 4B).

Fig 4B predicts also a variable differentiation rate during the experiment. In developmental systems, the balance between differentiative divisions and proliferative divisions has been shown to also change overtime [42, 14]. For instance, during motorneuron generation, the rate of differentiation has been shown to change sharply due to a sudden switch in Shh activity [42]. A similar scenario occurs *in vitro* in our system (see Fig. 4). When we inform our simulations with a variable differentiation rate, we observe that again both cumulative methods fail and show high dispersion between independent samples (Supp Fig 4C). The same occurs when both mode and rate of division are allowed to change simultaneously, as in our experiments (Supp Fig 4D).

In conclusion, our simulations show that the cumulative curves are not ideal when used to characterize the systems where proliferation and differentiation rate are variable. This fact, together with the reported effect of

BrdU and analogs in lengthening the cell cycle, could explain the different predictions between cumulative and branching process for our experiments.

3. Discussion

A detailed analysis of the dynamics of vertebrate neurogenesis involves a careful characterization of the features that regulate the dynamics of proliferation and differentiation of RG during the generation of the mammalian cortex. One of its most striking features is the fact that RG are restricted to an asymmetric mode of division *in vivo*, in contrast to other developmental systems [42, 14, 15, 16, 17, 18, 19, 20].

Our study suggests that RG are not restricted to an asymmetric mode of division when cultured *in vitro*. On the contrary, the mode of division seems to be dependent on the culture conditions. Several authors propose that the mode of division is modulated by the distribution of cell fate determinants during mitosis, the orientation of the spindle or the inheritance of the primary cilium or the different centrosomes [4]. It is possible that the apical-basal polarized structure of the RG, or their organization and orientation of the radial processes along the stratified neuroephitelium results in asymmetric inheritance of these cell fate regulators [4]. The loss of these features provided by the niche when cells are cultured *in vitro* may result in a probabilistic scenario where each of the 3 modes of divisions is possible, similarly to neuronal progenitor cells and other developmental systems [42, 14, 15, 16, 17, 18, 19, 20].

In these situations, the branching process framework is able to estimate the rates of each of the three modes of division [14]. This prediction for

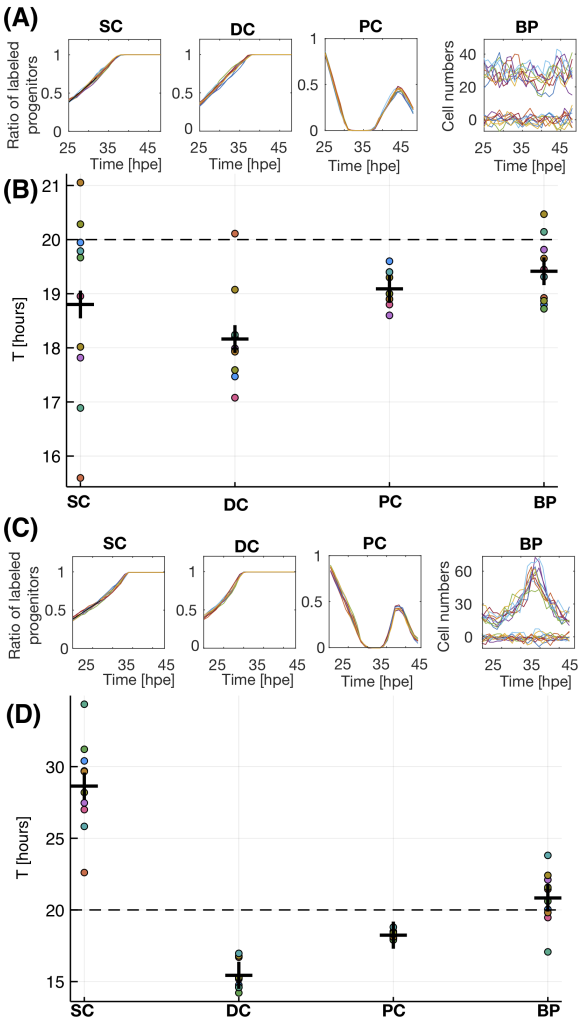

Figure 6: **Simulations explain the difference in cell cycle length calculated by EdU and Branching process.** (A,C) Cumulative curves generated numerically for each protocol for 10 independent runs of the model. (B,D) Quantification of T for each simulation (dots) and average (crosses). Each color corresponds to the same simulation analyzed using each framework. A-B correspond to conditions of constant cell cycle. C-D correspond to conditions of variable cell cycle.

the case of RG in culture is shown in Fig. 4E-F, where we can see that the predominant mode of division is *pp* (green). This symmetric mode of division is even more probable in conditions of +FGF, to the expenses of a reduction in *pd* and *dd*. A scheme that illustrates our findings is shown in Fig 5C. In brief, the single mode of division observed *in vivo* contrast with the probabilistic scenario observed *in vitro*, where all modes of division are possible. Changes in the culture conditions can shift the balance between the three modes of division, and increase the rate of *pp* divisions to the expenses of the other modes.

To rule out the possibility that a reduced number of neuroepithelial progenitors in the culture (that proliferate only via *pp*) are responsible for the generation of new RG, we performed immunofluorescence against Pax6, a well characterized marker for RG [53] that is not present in neuroepithelial progenitors [54]. Automated quantification is shown in Supp Fig 5, where around 100% of all Sox2 positive progenitors are also positive for Pax6 (so, there is no neuroepithelial progenitors at this stage in the culture, in agreement with the in *in vivo* data [3]). Another possibility is the presence of intermediate progenitors [55] that divide once to produce two terminally differentiated neurons [56]. Immunofluorescence against Tbr2, a marker for intermediate progenitors shows that no Tbr2 positive cells in the culture in the two culture conditions tested (data not shown). This is probably due to the fact that FGF has been shown to inhibit the transition from RG to intermediate progenitor [57] (FGF is in the culture media in both control and +FGF conditions).

A detailed analysis of the dynamics of vertebrate neurogenesis involves a

careful characterization of the rate of division. The most direct method to measure the cell cycle length requires to monitor the time between consecutive mitotic evens at single cell resolution [58]. Unfortunately, due to the high degree of variability, many cells in a population need to be sampled, segmented and tracked simultaneously to obtain an accurate value, even when dealing with clonal samples [59].

Indirect methods based on cumulative incorporation of thymidine analogs perform well in conditions of constant proliferation and differentiation, but they are not designed to study systems where the cell cycle changes overtime, which is is potentially the case in many developmental systems. In these conditions, the Branching Process formalism and the Pulse-Chase outperform cumulative curve methods. On the other hand, the Pulse-Chase method requires experiments that are longer that cell cycle length. Therefore, the effect of the labeling agent for long periods of time may affect strongly the normal cell cycle progression [31, 30]. A clear advantage of the Branching Process is that it does not involve manipulation of the samples before fixation, so there is no interference with the normal progression of the cell cycle. In addition, the Branching Process formalism also provides the correct value of T with temporal resolution, and the measurement of the average differentiation rate, (also with temporal resolution).

Several studies have shown that the length of G1 phase increases progressively when neurogenesis starts, resulting in a overall increase of the cell cycle [44, 45, 46, 47, 48, 49]. Alternatively, others studies show that the cell cycle length is shorter in neurogenic divisions, compared to proliferative divisions [50, 42, 43, 51, 52], due mainly to a shortening in S-phase. Our results

show that FGF promotes pp divisions and shortens cell cycle, consistent with the hypothesis that proliferative divisions have a shorter cell cycle, maybe via a shortening of G1-phase (similarly to insulin-like growth factor [60, 61]). A careful characterization of how FGF affects each phase of the cell cycle it is far from the scope of this contribution.

In addition, our data also shows an increase in the growth fraction γ in conditions of extra FGF compared to control, when monitoring the cycling progenitors using Ki67 staining (Supp Fig 2C-D), in agreement with previous studies [62]. Interestingly, this is not shown in the cumulative curve estimation, maybe due to the fact that the growth fraction seems to be also changing during the experiment (Supp Fig 2C-D).

The culture and differentiation of RG cells *in vitro* provides a very good framework to study basic features that orchestrate the formation of the mammalian neocortex. In brief, the system provides a well controlled environment where the effect of signaling molecules and other conditions can be tested reliably, while providing easier manipulation and imaging compared to studies performed *in vivo*. We use this framework to study the features that restrict the division mode of RG as deterministic versus the more common probabilistic scenario observed in many other scenarios. Our combined experimental/computational/theoretical approach can be also used to test the effect of other signaling networks by quantifying the cell cycle and mode after small molecule inhibition and comparison with the control culture.

4. References

[1] S. Lodato, P. Arlotta, Generating neuronal diversity in the mammalian cerebral cortex., Annual Review of Cell and Developmental Biology 31 (2015) 699–720.

[2] F. Matsuzaki, A. Shitamukai, Cell division modes and cleavage planes of neural progenitors during mammalian cortical development., Cold Spring Harbor Perspectives in Biology 7 (2015) a015719.

[3] R. Beattie, S. Hippenmeyer, Mechanisms of radial glia progenitor cell lineage progression., FEBS Letters 591 (2017) 3993–4008.

[4] E. Taverna, M. Gtz, W. B. Huttner, The cell biology of neurogenesis: toward an understanding of the development and evolution of the neocortex., Annual Review of Cell and Developmental Biology 30 (2014) 465–502.

[5] K. Frederiksen, R. D. McKay, Proliferation and differentiation of rat neuroepithelial precursor cells in vivo., The Journal of Neuroscience 8 (1988) 1144–1151.

[6] E. Hartfuss, R. Galli, N. Heins, M. Gtz, Characterization of CNS precursor subtypes and radial glia., Developmental Biology 229 (2001) 15–30.

[7] T. Miyata, A. Kawaguchi, H. Okano, M. Ogawa, Asymmetric inheritance of radial glial fibers by cortical neurons., Neuron 31 (2001) 727–741.

[8] S. C. Noctor, V. Martnez-Cerdeo, L. Ivic, A. R. Kriegstein, Cortical neurons arise in symmetric and asymmetric division zones and migrate through specific phases., Nature Neuroscience 7 (2004) 136–144.

[9] R. Losick, C. Desplan, Stochasticity and cell fate., Science 320 (2008) 65–68.

[10] J. Teles, C. Pina, P. Edn, M. Ohlsson, T. Enver, C. Peterson, Transcriptional regulation of lineage commitment–a stochastic model of cell fate decisions., PLoS Computational Biology 9 (2013) e1003197.

[11] C. E. Mller-Sieburg, R. H. Cho, M. Thoman, B. Adkins, H. B. Sieburg, Deterministic regulation of hematopoietic stem cell self-renewal and differentiation., Blood 100 (2002) 1302–1309.

[12] Y. Kosodo, K. Rper, W. Haubensak, A.-M. Marzesco, D. Corbeil, W. B. Huttner, Asymmetric distribution of the apical plasma membrane during neurogenic divisions of mammalian neuroepithelial cells., The EMBO Journal 23 (2004) 2314–2324.

[13] W. B. Huttner, Y. Kosodo, Symmetric versus asymmetric cell division during neurogenesis in the developing vertebrate central nervous system., Current Opinion in Cell Biology 17 (2005) 648–657.

[14] D. G. Mguez, A branching process to characterize the dynamics of stem cell differentiation., Scientific reports 5 (2015) 13265.

[15] J. He, G. Zhang, A. D. Almeida, M. Cayouette, B. D. Simons, W. A. Harris, How variable clones build an invariant retina., Neuron 75 (2012) 786–798.

[16] Z. Chen, X. Li, C. Desplan, Deterministic or stochastic choices in retinal neuron specification., Neuron 75 (2012) 739–742.

[17] E. Clayton, D. P. Doup, A. M. Klein, D. J. Winton, B. D. Simons, P. H. Jones, A single type of progenitor cell maintains normal epidermis., Nature 446 (2007) 185–189.

[18] V. H. Teixeira, P. Nadarajan, T. A. Graham, C. P. Pipinikas, J. M. Brown, M. Falzon, E. Nye, R. Poulsom, D. Lawrence, N. A. Wright, S. McDonald, A. Giangreco, B. D. Simons, S. M. Janes, Stochastic homeostasis in human airway epithelium is achieved by neutral competition of basal cell progenitors., eLife 2 (2013) e00966.

[19] A. M. Klein, T. Nakagawa, R. Ichikawa, S. Yoshida, B. D. Simons, Mouse germ line stem cells undergo rapid and stochastic turnover., Cell Stem Cell 7 (2010) 214–224.

[20] H. J. Snippert, L. G. van der Flier, T. Sato, J. H. van Es, M. van den Born, C. Kroon-Veenboer, N. Barker, A. M. Klein, J. van Rheenen, B. D. Simons, H. Clevers, Intestinal crypt homeostasis results from neutral competition between symmetrically dividing lgr5 stem cells., Cell 143 (2010) 134–144.

[21] P. Gao, M. P. Postiglione, T. G. Krieger, L. Hernandez, C. Wang, Z. Han, C. Streicher, E. Papusheva, R. Insolera, K. Chugh, O. Kodish, K. Huang, B. D. Simons, L. Luo, S. Hippenmeyer, S.-H. Shi, Deterministic progenitor behavior and unitary production of neurons in the neocortex., Cell 159 (2014) 775–788.

[22] L. G. W. Hilgenberg, M. A. Smith, Preparation of dissociated mouse cortical neuron cultures., Journal of Visualized Experiments (2007) 562.

[23] R. S. Nowakowski, S. B. Lewin, M. W. Miller, Bromodeoxyuridine immunohistochemical determination of the lengths of the cell cycle and the DNA-synthetic phase for an anatomically defined population., Journal of Neurocytology 18 (1989) 311–318.

[24] A. Salic, T. J. Mitchison, A chemical method for fast and sensitive detection of DNA synthesis in vivo., Proceedings of the National Academy of Sciences of the United States of America 105 (2008) 2415–2420.

[25] S. B. Buck, J. Bradford, K. R. Gee, B. J. Agnew, S. T. Clarke, A. Salic, Detection of s-phase cell cycle progression using 5-ethynyl-2'-deoxyuridine incorporation with click chemistry, an alternative to using 5-bromo-2'-deoxyuridine antibodies., Biotechniques 44 (2008) 927–929.

[26] M. R. Alexiades, C. Cepko, Quantitative analysis of proliferation and cell cycle length during development of the rat retina., Developmental Dynamics 205 (1996) 293–307.

[27] M. Takahashi, Theoretical basis for cell cycle analysis i. labelled mitosis wave method, Journal of Theoretical Biology 13 (1966) 202–211.

[28] T. Takahashi, R. S. Nowakowski, V. S. Caviness, The leaving or q fraction of the murine cerebral proliferative epithelium: a general model of neocortical neuronogenesis., The Journal of Neuroscience 16 (1996) 6183–6196.

[29] P. D. M. Macdonald, Statistical inference from the fraction labelled mitoses curve, Biometrika 57 (1970) 489–503.

[30] J. Duque, N. Gorfinkiel, Integration of actomyosin contractility with cell-cell adhesion during dorsal closure., Development 143 (2016) 4676–4686.

[31] L. H. Levkoff, G. P. Marshall, H. H. Ross, M. Caldeira, B. A. Reynolds, M. Cakiroglu, C. L. Mariani, W. J. Streit, E. D. Laywell, Bromodeoxyuridine inhibits cancer cell proliferation in vitro and in vivo., Neoplasia 10 (2008) 804–816.

[32] C. B. Johansson, S. Momma, D. L. Clarke, M. Risling, U. Lendahl, J. Frisn, Identification of a neural stem cell in the adult mammalian central nervous system., Cell 96 (1999) 25–34.

[33] A. C. Begg, N. J. McNally, D. C. Shrieve, H. Krcher, A method to measure the duration of DNA synthesis and the potential doubling time from a single sample., Cytometry 6 (1985) 620–626.

[34] M. Hoyer, S. M. Bentzen, L. N. Salling, J. Overgaard, Influence of sampling time on assessment of potential doubling time, Cytometry 16 (1994) 144–151.

[35] M. C. Johansson, B. Baldetorp, P. O. Bendahl, R. Johansson, S. M. Oredsson, An improved mathematical method to estimate DNA synthesis time of bromodeoxyuridine-labelled cells, using FCM-derived data, Cell Proliferation 27 (1994) 475–488.

[36] T. S. Weber, I. Jaehnert, C. Schichor, M. Or-Guil, J. Carneiro, Quantifying the length and variance of the eukaryotic cell cycle phases by a stochastic model and dual nucleoside pulse labelling., PLoS Computational Biology 10 (2014) e1003616.

[37] H. Y. Lee, A. S. Perelson, Modeling t cell proliferation and death in vitro based on labeling data: generalizations of the smith-martin cell cycle model., Bulletin of Mathematical Biology 70 (2008) 21–44.

[38] A. Zilman, V. V. Ganusov, A. S. Perelson, Stochastic models of lymphocyte proliferation and death., Plos One 5 (2010).

[39] M. A. Ritter, J. F. Fowler, Y. Kim, M. J. Lindstrom, T. J. Kinsella, Single biopsy, tumor kinetic analyses: A comparison of methods and an extension to shorter sampling intervals, International Journal of Radiation Oncology*Biology*Physics 23 (1992) 811–820.

[40] P. Taupin, BrdU immunohistochemistry for studying adult neurogenesis: paradigms, pitfalls, limitations, and validation., Brain Research Reviews 53 (2007) 198–214.

[41] S. Shibui, T. Hoshino, M. Vanderlaan, J. W. Gray, Double labeling with iodo- and bromodeoxyuridine for cell kinetics studies., The Journal of Histochemistry and Cytochemistry 37 (1989) 1007–1011.

[42] M. Saade, I. Gutirrez-Vallejo, G. Le Drau, M. A. Rabadn, D. G. Miguez, J. Buceta, E. Mart, Sonic hedgehog signaling switches the mode of division in the developing nervous system., Cell reports 4 (2013) 492–503.

[43] G. Le Drau, M. Saade, I. Gutirrez-Vallejo, E. Mart, The strength of SMAD1/5 activity determines the mode of stem cell division in the developing spinal cord., The Journal of Cell Biology 204 (2014) 591–605.

[44] T. Takahashi, R. S. Nowakowski, V. S. Caviness, The cell cycle of the pseudostratified ventricular epithelium of the embryonic murine cerebral wall., The Journal of Neuroscience 15 (1995) 6046–6057.

[45] F. Calegari, W. B. Huttner, An inhibition of cyclin-dependent kinases that lengthens, but does not arrest, neuroepithelial cell cycle induces premature neurogenesis., Journal of Cell Science 116 (2003) 4947–4955.

[46] F. Calegari, W. Haubensak, C. Haffner, W. B. Huttner, Selective lengthening of the cell cycle in the neurogenic subpopulation of neural progenitor cells during mouse brain development., The Journal of Neuroscience 25 (2005) 6533–6538.

[47] C. Dehay, H. Kennedy, Cell-cycle control and cortical development., Nature Reviews. Neuroscience 8 (2007) 438–450.

[48] G. Mairet-Coello, A. Tury, E. Van Buskirk, K. Robinson, M. Genestine, E. DiCicco-Bloom, p57(KIP2) regulates radial glia and intermediate precursor cell cycle dynamics and lower layer neurogenesis in developing cerebral cortex., Development 139 (2012) 475–487.

[49] M. Roccio, D. Schmitter, M. Knobloch, Y. Okawa, D. Sage, M. P. Lutolf, Predicting stem cell fate changes by differential cell cycle progression patterns., Development 140 (2013) 459–470.

[50] Y. Arai, J. N. Pulvers, C. Haffner, B. Schilling, I. Nsslein, F. Calegari, W. B. Huttner, Neural stem and progenitor cells shorten s-phase on commitment to neuron production., Nature Communications 2 (2011) 154.

[51] A. Iulianella, M. Sharma, M. Durnin, G. B. Vanden Heuvel, P. A. Trainor, Cux2 (cutl2) integrates neural progenitor development with cell-cycle progression during spinal cord neurogenesis., Development 135 (2008) 729–741.

[52] M. Locker, M. Agathocleous, M. A. Amato, K. Parain, W. A. Harris, M. Perron, Hedgehog signaling and the retina: insights into the mechanisms controlling the proliferative properties of neural precursors., Genes & Development 20 (2006) 3036–3048.

[53] D. M. Suter, D. Tirefort, S. Julien, K.-H. Krause, A sox1 to pax6 switch drives neuroectoderm to radial glia progression during differentiation of mouse embryonic stem cells., Stem Cells 27 (2009) 49–58.

[54] G. E. Elsen, F. Bedogni, R. D. Hodge, T. K. Bammler, J. W. MacDonald, S. Lindtner, J. L. R. Rubenstein, R. F. Hevner, The epigenetic factor landscape of developing neocortex is regulated by transcription factors pax6 tbr2 tbr1., Frontiers in Neuroscience 12 (2018) 571.

[55] B. J. Molyneaux, P. Arlotta, J. R. L. Menezes, J. D. Macklis, Neuronal subtype specification in the cerebral cortex., Nature Reviews. Neuroscience 8 (2007) 427–437.

[56] S. R. Hutton, L. H. Pevny, SOX2 expression levels distinguish between neural progenitor populations of the developing dorsal telencephalon., Developmental Biology 352 (2011) 40–47.

[57] W. Kang, L. C. Wong, S.-H. Shi, J. M. Hbert, The transition from radial glial to intermediate progenitor cell is inhibited by FGF signaling during corticogenesis., The Journal of Neuroscience 29 (2009) 14571–14580.

[58] A. Sigal, R. Milo, A. Cohen, N. Geva-Zatorsky, Y. Klein, Y. Liron, N. Rosenfeld, T. Danon, N. Perzov, U. Alon, Variability and memory of protein levels in human cells., Nature 444 (2006) 643–646.

[59] O. Sandler, S. P. Mizrahi, N. Weiss, O. Agam, I. Simon, N. Q. Balaban, Lineage correlations of single cell division time as a probe of cell-cycle dynamics., Nature 519 (2015) 468–471.

[60] G. Mairet-Coello, A. Tury, E. DiCicco-Bloom, Insulin-like growth factor-1 promotes g(1)/s cell cycle progression through bidirectional regulation of cyclins and cyclin-dependent kinase inhibitors via the phosphatidylinositol 3-kinase/akt pathway in developing rat cerebral cortex., The Journal of Neuroscience 29 (2009) 775–788.

[61] R. D. Hodge, A. J. D'Ercole, J. R. O'Kusky, Insulin-like growth factor-i accelerates the cell cycle by decreasing g1 phase length and increases cell cycle reentry in the embryonic cerebral cortex., The Journal of Neuroscience 24 (2004) 10201–10210.

[62] S. Bouleau, H. Grimal, V. Rincheval, N. Godefroy, B. Mignotte, J.-L.

Vayssire, F. Renaud, FGF1 inhibits p53-dependent apoptosis and cell cycle arrest via an intracrine pathway., Oncogene 24 (2005) 7839–7849.

[63] J. Schindelin, I. Arganda-Carreras, E. Frise, V. Kaynig, M. Longair, T. Pietzsch, S. Preibisch, C. Rueden, S. Saalfeld, B. Schmid, J.-Y. Tinevez, D. J. White, V. Hartenstein, K. Eliceiri, P. Tomancak, A. Cardona, Fiji: an open-source platform for biological-image analysis., Nature Methods 9 (2012) 676–682.

[64] H. Kang, S. H. Lee, J. Lee, Image segmentation based on fuzzy flood fill mean shift algorihm, in: 2010 Annual Meeting of the North American Fuzzy Information Processing Society, IEEE, 2010, pp. 1–6.

[65] H. Harrison, H. J. Pegg, J. Thompson, C. Bates, P. Shore, HIF1-alpha expressing cells induce a hypoxic-like response in neighbouring cancer cells., BMC Cancer 18 (2018) 674.

[66] K. Len, J. Faro, J. Carneiro, A general mathematical framework to model generation structure in a population of asynchronously dividing cells., Journal of Theoretical Biology 229 (2004) 455–476.

[67] P. L. Martinez-Morales, A. C. Quiroga, J. A. Barbas, A. V. Morales, SOX5 controls cell cycle progression in neural progenitors by interfering with the WNT-beta-catenin pathway., EMBO Reports 11 (2010) 466–472.

[68] F. Dolbeare, J. R. Selden, Immunochemical quantitation of bromodeoxyuridine: application to cell-cycle kinetics., Methods in Cell Biology 41 (1994) 297–316.

[69] J. A. Bradford, S. T. Clarke, Dual-pulse labeling using 5-ethynyl-2'-deoxyuridine (EdU) and 5-bromo-2'-deoxyuridine (BrdU) in flow cytometry., Current protocols in cytometry / editorial board, J. Paul Robinson, managing editor ... [et al.] Chapter 7 (2011) Unit 7.38.

[70] V. Graham, J. Khudyakov, P. Ellis, L. Pevny, SOX2 functions to maintain neural progenitor identity., Neuron 39 (2003) 749–765.

[71] D. G. Mguez, Network nonlinearities in drug treatment., Interdisciplinary sciences : computational life sciences 5 (2013) 85–94.

[72] T. Scholzen, J. Gerdes, The ki-67 protein: from the known and the unknown., Journal of Cellular Physiology 182 (2000) 311–322.

[73] G. B. Blanchard, S. Murugesu, R. J. Adams, A. Martinez-Arias, N. Gorfinkiel, Cytoskeletal dynamics and supracellular organisation of cell shape fluctuations during dorsal closure., Development 137 (2010) 2743–2752.

5. Methods

5.1. Preparation of dissociated mouse cortical neuron cultures and cell culturing

Cortical neurons and neural progenitors were obtained from E11/E11.5 mouse embryos of the C57 BL/6JRCC strain, as previously described in Ref. [22]. Briefly, meninges were carefully removed and after the isolation of the cortex from all embryos, these were incubated in Hank's Buffered Salt Solution free of Ca2+ and Mg2+ (HBSS, ThermoFisher 14185) and mechanically

disaggregated using Pasteur pipettes. Cells were plated in glasses treated with Nitric Acid and Fibronectin at 10 g/ml (Fisher Scientific; 15602707) to maximize cell adhesion, using as standard medium Neurobasal without L-glutamine (ThermoFisher 21103-049) and: Glutamax (ThermoFisher 35050-038); B-27 (ThermoFisher 17504-044); 0.02 ng/μl of recombinant murine EGF (PeproTech 315-09, lot number 0517179-1); 0.02 ng/μl of human FGF basic (PreproTech 100-18B, lot number 0311706-1); and Penicillin, Streptomycin and Antimicotic (concentrations standard for cell culture). Cells were plated at constant density (250000 cells in each M24 well) for all experiments. After 24 hours post-extraction (hpe) to allow for recovery post extraction, half of the culture media is removed and replaced with standard media (control conditions) standard media complemented with human FGF basic for a final concentration of 0.06 ng/μ (+FGF conditions). All experimental protocols were in accordance with the guidelines of the European Communities Directive (2012/63UE) and the actual Spanish legislation (RD 53/2013).

5.2. Immunofluorescence and cells mounting

Cells were fixed for 20 minutes at Room Temperature (RT) with 4% paraformaldehyde and washed twice for 5 minutes with Phosphate Buffer Saline (PBS) 1X. Fixed cells were incubated with a permeabilization solution composed of triton (ChemSupply 9002-93-1) at 0.6% in PBS 1X for 20 minutes at RT. Next, cells were washed 3 times with PBS 1X. Next, blocking solution is added (Bovine Serum Albumin, BSA. Sigma ;A7906) at 3% in PBS 1X for at least 30 minutes. Later, cells were incubated with primary antibodies dissolved in the blocking solution overnight at 4C. The next day, cells were washed with PBS 1X 3-4 times, for 5 minutes for each one, and they

were incubated with secondary antibodies in the blocking solution for 45 minutes at RT, protected from light. Then, secondary antibodies were removed, and nuclei were stained with Hoechst 3342 (1/2000, ThermoFisher 1399) dissolved in PBS 1X for 5 minutes at RT. Finally, the cells were washed in PBS 1X, double distilled water, and ethanol at 70% and, after, the coverslips with the cells were mounted with Fluoromount G (Southern Biotechnology Associates, Inc, Birmingham, Alabama 0100-01) on microscope glass slides.

Primary antibodies used were: anti-Sox2 (1/2000, GeneTex GTX124477), anti-Map2 (1/200, Santa Cruz Biotechnology sc-74421); anti-Pax6 (1/1000, BioLegend B244573); anti-Cleaved Caspase 3 (1/1000, Cell Signaling 9661); and anti-KI67 (1/200, ThermoFisher 14-5698-82). Secondary antibodies used were: anti-Rabbit 488 (1/1000, ThermoFisher A-21206) and anti-Mouse 555 (1/1000, ThermoFisher A-21137) and anti-Rat 555 (1/1000, ThermoFisher A-21434).

5.3. Image acquisition and analysis

Samples were imaged in a confocal microscope AR1+ of high speed in acquisition and sensibility coupled to an inverted microscope model Eclipse Ti-E (Nikon) with a 20X objective and a resolution of 1024x1024 pixels. Image processing has been conducted with the free software Fiji [63], using implemented algorithms and in house developed computational routines. The software allows us to monitor a large number of cells per condition (around 10^5 cells per experiment) to minimize the effect of variability and heterogeneity in each sample. A number of cells in the culture are simultaneously Sox2- and Map2-, and have a nucleus that is substantially larger that Sox2+ or Map2+. This cells are considered non RG or differentiated neurons, and

are not quantified by our script. In brief, image processing and analysis designed routines for the identification and classification of cells were based on the segmentation of nuclei and the classification of each nuclei based on fluorescent intensity in each channel. The sequence of processing algorithms and filters is as follows.

1. Definition of the Kernel Radius (KR) used by several of the filters in the framework. The KR defines the portion of the image used for calculations and processing of the filters. KR was fixed as 2.5.

2. Local increment of differences between the foreground and background intensities applying a local kernel window of size 8xKRxKR that was moving across the image, removing all pixels with a value less than the median of each local kernel window.

3. The previous filter separates adjacent objects, but also generates holes and breaks the integrity of objects. To solve it, the following sequence of filters is applied to remove noise and increase the definition of the boundaries of each object: Gaussian Blur filter, Maximum Filter, Median filter and Unsharp Mask filter.

4. Thresholding was performed using as cutoff value the median value calculated from all intensity values from the image higher than zero.

5. Euclidean Distance Map (EDT) was performed in the binary image to generate the primordium points (seeds) for all detected objects. Later, using the seeds a flood fill algorithm was applied to find the boundaries of each object [64].

6. Finally, image analysis of all objects was performed using Fiji [63]. All segmented objects were fitted to ellipses using standard tools from Fiji. Objects smaller than KR^*KR are discarded from the analysis.

Due to the specific features of each staining, a different set of processing filters is applied to remove background and noise for each channel.

- Map2: Double sequential thresholding to extract foreground information (cutoff 1 = mean, cutoff 2: median); morphological opening to remove neurons fibers (structuring element: lines at different angle with a length of 2xKR); Gaussian filter to remove noise (radius=KR).

- Sox2: Double sequential thresholding to extract foreground information (cuttof 1, = mean, cutoff 2: median); morphological opening to select only nuclei with minimal size (structuring element: circumference of radius equal to 2xKR); Gaussian filter to remove noise (radius=KR).

- EdU: Single thresholding to extract foreground information (cutoff = median); morphological opening (structuring element: circumference of radius equal to 2xKR); Gaussian filter to remove noise (radius=KR).

- Pax6: Single thresholding to extract foreground information (cutoff = mean); morphological opening (structuring element: circumference of radius equal to 2xKR); Gaussian filter to remove noise (radius=KR).

- Cleaved Caspase-3: Double sequential thresholding to extract foreground information (cutoff 1= mean, cutoff 2 = mean + plus standard deviation); morphological opening to select only nuclei with minimal size

(structuring element: circumference of radius equal to 2xKR); Gaussian filter to remove noise (radius=KR).

- Ki67: Single thresholding to extract foreground information (cutoff = mean); morphological opening (structuring element: circumference of radius equal to 2xKR); Gaussian filter to remove noise (radius=KR).

Finally, the fitted **ellipse** for each nucleus was used to identify the fate of each cell. To do that, ellipses were overlapped in the image of each marker, and the phenotype was assigned attending to the area with pixels values higher than zero comparing between images of used markers. For the MAP-2, area was set to at least 15%, and 1% for the rest.

5.4. Statistical and Data analysis

P values were calculated assuming that both samples follows a students t distribution. Cell cycle values in Fig. 2C-D were obtained after linear regression of the four first data points. Rates of quiescence in Fig. 2C-D were obtained after linear regression of the four last points. Three-parameter sigmoidal fitting was used to fit data from fig. 3B-C (slope was adjusted manually). Sample size for all experiments is at least 4. Fittings and statistical analysis were performed using Matlab© algorithms and scripts (The Mathworks©, Natick, MA).

5.5. EdU cumulative curve

Cumulative curve of the thymidine analog 5-Ethynyl-2'-deoxyUridine (EdU) incorporation was performed using Click-iT™ Plus EdU Alexa Fluor™ 647 Imaging Kit (ThermoFisher; C10640). Briefly, EdU was added around 24 hpe

at 2 μM. Cells were then fixed at increasing times of EdU exposition. Staining of EdU positive cell was performed based on previously published protocols [65]. Next, immunostaining against Sox2 is used as standard marker for RG progenitors [3]. Later, the number of cells positive simultaneously for Sox2 and EdU was quantified in all time points using automated image processing. To calculate the cell cycle length, the percentage of progenitor cells that have incorporated EdU was plotted against the hours of EdU incorporation. The saturation value at long incubation times was used to calculate the growth fraction γ. This value is then used to calculate the average cell cycle using linear regression at short EdU accumulation times (see figure 2).

5.6. EdU pulse-and-chase experiments.

Cells were exposed to a short pulse of 30 minutes of EdU at 36 hpe. Pulse points were fixed at this time pont. Chase points were washed three times with fresh medium, and fixed 15 hours after the pulse. Later, the number of EdU positive/Sox2 positive cells were quantified in both pulse and chase time points for both conditions using automated image processing.

5.7. Numerical simulations of cell populations.

We developed an *in silico* model of the culture of cells as numerical entities that proliferate, differentiate enter quiescence or apoptosis according to probabilities established by the user. An initial set of un-synchronized progenitors cells are allowed to cycle following the different phases of the cell cycle: from G_1 to S to G_2 to finally M phase. Upon division, the tow resulting daughter cells either remain as progenitors (*pp* division), they become

terminally differentiated cells and stop cycling (*dd* division), or one remains as progenitor while the other differentiates (*pd* division).

A scheme of how the population is defined and develops overtime is shown in Supp Fig 1. Parameters of the simulation are: the number of initial cells m, the average cell cycle T at each time point (defined as $T = \sum T^i/n$, being n the number of cells at time t), the fraction of cycling progenitors (or growth fraction) γ, the rate of apoptosis of progenitors $\emptyset_P$, and the length of the experiment t_{end}. The age of each cell is defined as the time since its birth, and the type corresponds to its characteristic as progenitors (P, cycling cells), differentiated (D, non cycling cells), quiescent (Q, non cycling progenitors) and apoptotic (dying cells).

For simplicity, the cell cycle is divided into just three main steps of equal length: G_1, followed by S and finally followed by $G_2 + M$. ($T = T_{G1} + T_S + T_{G2M}$). Changes in the cell cycle length affect all phases of the cell cycle identically (simulations where the phases are of different length and that changes affecting differently different phases of the cell cycle show equivalent results). The value for each parameter is obtained from a gamma distribution with mean defined by the user and standard deviation of 30% of the mean, to mimic variability in a clonal population [66].

5.8. Simulations of Cell Cycle determination methods

The previous model is then adapted to perform a computational analog of one or two thimidine compounds. At any time in the simulation, EdU can be added to the cells, so cells undergoing S-phase will be labeled as "positive", and will remain as positive throughout the rest of the simulation. The input parameters of the model are varied to simulate different dynamics of

a population of cells in different conditions, in terms of quiescence, apoptosis, cell cycle length and differentiation rate. For each condition tested, we will perform four measurements of the cell cycle based on the following methodologies:

Cumulative Curve method.

This technique has been extensively used both in *in vitro* and *in vivo* situations to quantify the rate of cells in the population entering S-phase [67, 43]. A scheme of the method is shown in Supp Fig 3A. In brief, a nucleoside analog is added to several identical samples that are fixed and stained at different times. Labeled cells in all samples are quantified using microscopy or flow-cytometry. The ratio of progenitor cells that are labeled for each sample is plotted, and the values corresponding to the cell cycle length T are obtained from the slope of a linear regression fitting of the data at short exposure times. In addition, the fraction of cycling progenitor cells γ, or growth fraction, can be estimated from the rate of labeled cells after long exposure times. This method, when combined with dyes to measure DNA content can be used to determined the length of the different phases of the cell cycle [68].

Dual Cumulative Curve Method. This method combines dual staining with thymidine analogs [24]. It also provides the possibility of fixing all samples simultaneously to ensure that quantification is performed always at the same developmental time. In addition, it can also provide some positional information of regions in a given tissue where cells cycle at different rates [41, 69]. On the other hand, it requires a more complex experimental design, and it may also result in increased toxicity. In addition, it does not

provide information about the growth fraction. The method (Supp Fig 3B) involves a first labelling agent administered to all samples simultaneously, and a second agent administered at different time points. All samples are collected at the same time, and they are stained for both labelling agents. The amount or cells that are double positive overtime for the two different thymine analogs is plotted, and the average length of T and T_S can be extracted using linear or nonlinear regression (some corrections regarding the potential differential incorporation of both agents are required).

Pulse-Chase method. Both previous methods rely on long term exposure of the samples to nucleoside analogs, which can result in toxicity effects. Alternative, a short pulse can be also applied [36] to label only cells that where in S-phase at a given time. Then, the population of positive cells is "chased" in the different samples by fixing and staining at different times. Several variations of this method have been developed. A commonly used technique is to stain cells in mitosis (using immunofluorescence against phospho-histone-3), or using a second thymine analog in S-phase to chase cells that have re-entered in a new S-phase. A scheme of the method is shown in Supp Fig 3C.

The ratio of double positive cells in the different samples is plotted overtime, and the average value of T corresponds to the time between the pulse and the maximum of double positive cells in the population. The slope of the curve at shorter time scales can be used to calculate the length of S-phase. Measurements of the cell cycle using this methods requires significantly longer experiments than the two previous methods.

Branching Process method

Our lab recently developed an alternative method based on quantification of the amount of proliferative, differentiated, quiescent and apoptotic cells in the population at different times. A scheme of the method is shown in Supp Fig 3D, and an example of its experimental implementation can be found in Ref. [14]. In brief, samples are allowed to develop without interfering with the normal dynamics of the cells, and then are fixed at different developmental times. After fixation, the amount of cells in each state is quantified by antibody staining to distinguish progenitor cells [70], differentiated cells [71], cycling cells [72] and apoptotic cells [73], while the growth fraction can be identified from the progenitor population using antibodies, such as the proliferation-related antigen Ki-67. This nuclear protein is present in the nuclei of cells in the G_1, S and G_2 phases of the cell cycle as well as in mitosis, but not in quiescent cells (cells in G_0) [72].

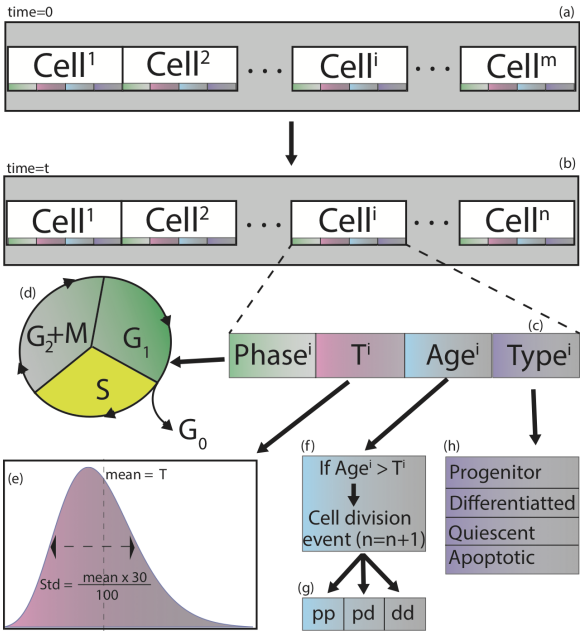

Figure 7: **Supplementary Figure 1: Scheme of the simulation of the population model.** In brief: (a) an initial number m of un-syncronized progenitor cells proliferates and differentiates. (b) At any given time t, each cell i in the population of n cells is characterised by four parameters (c): phase, T, age and Type. (d) Cells cycle in their phase from G_1 to S to $G_2 + M$. When a given cell i reaches the end of $G_2 + M$, a division event takes place, with three different outcomes (g): *pp*, *pd* or *dd* division. In the presence of a labelling agent, cells incorporate it only during S-phase, and become labeled as "positive" (showed in yellow). Depending on their type, cells are sorted into 4 groups (h): progenitors, differentiated, quiescent and apoptotic.

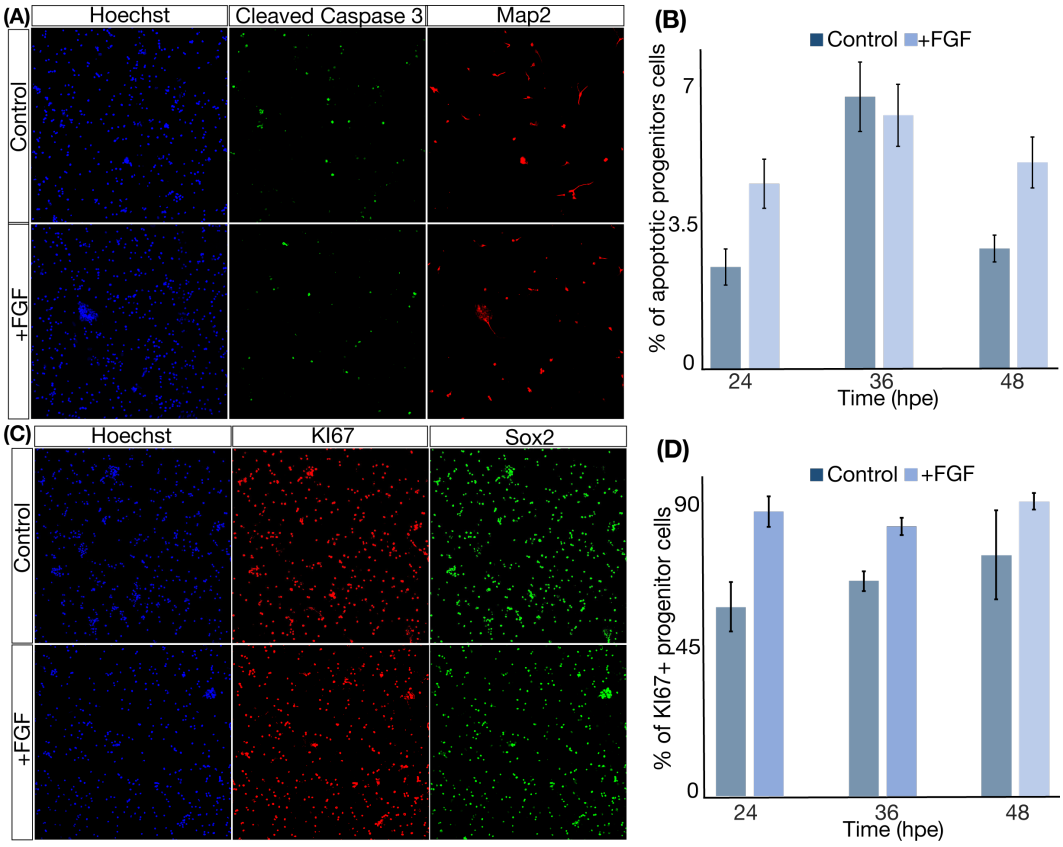

Figure 8: **Supplementary Figure 2: Experiments to obtain the growth fraction and apoptosis rate.** (A) Example of cells stained with nuclei (blue), cleaved Caspase3 (green), and Map2 (red) at 36 hpe. (B) Quantification of the percentage of progenitor cells that show positive staining for Caspase3 for both conditions and at three different time points. (C) Example of cells stained with nuclei (blue), KI67 (red) and Sox2 (green) at 36 hpe. (D) Quantification of the percentage of progenitor cells that are actively cycling both conditions and at three different time points. Columns represent the mean between independent quantifications. Error bars represent the standard error or the mean.

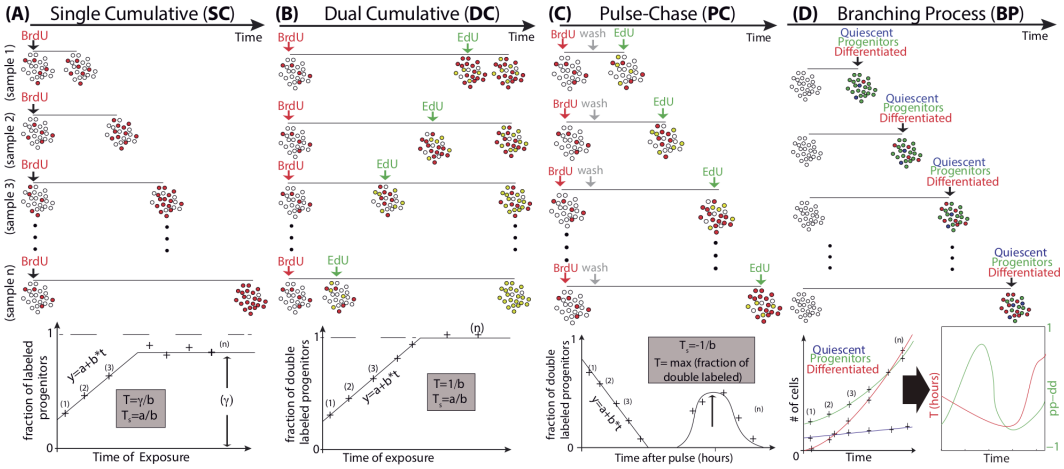

Figure 9: **Supplementary Figure 3: Scheme of methods tested to measure cell cycle length.** (A) Cumulative curve: A thymidine analog is added to all samples simultaneously. Samples are fixed at different times and stained for quantification. Linear fitting of the rate of labelling is used to determine the average T and γ_P. (B) Dual Cumulative: The first thymidine analog (red) is administered to all samples simultaneously. The second thymine analog (green) is administered at different times. All samples are then fixed simultaneously. Quantification of all double positive cells (yellow) is plotted against exposure time. This method does not provide an estimation of the growth fraction. (C) Pulse-chase: A short pulse of a first nucleoside analog is added to all samples simultaneously. A second nucleoside analog is added at different times, and the samples are fixed and stained immediately after. The amount of double positive cells is plotted overtime. (D) Branching process: Cells are fixed at different times and stained with antibodies to distinguish progenitors, differentiated, quiescent and apoptotic cells. The resulting numbers are used to inform the equations 1-2, that will give us the values of the average rate and mode of division overtime.

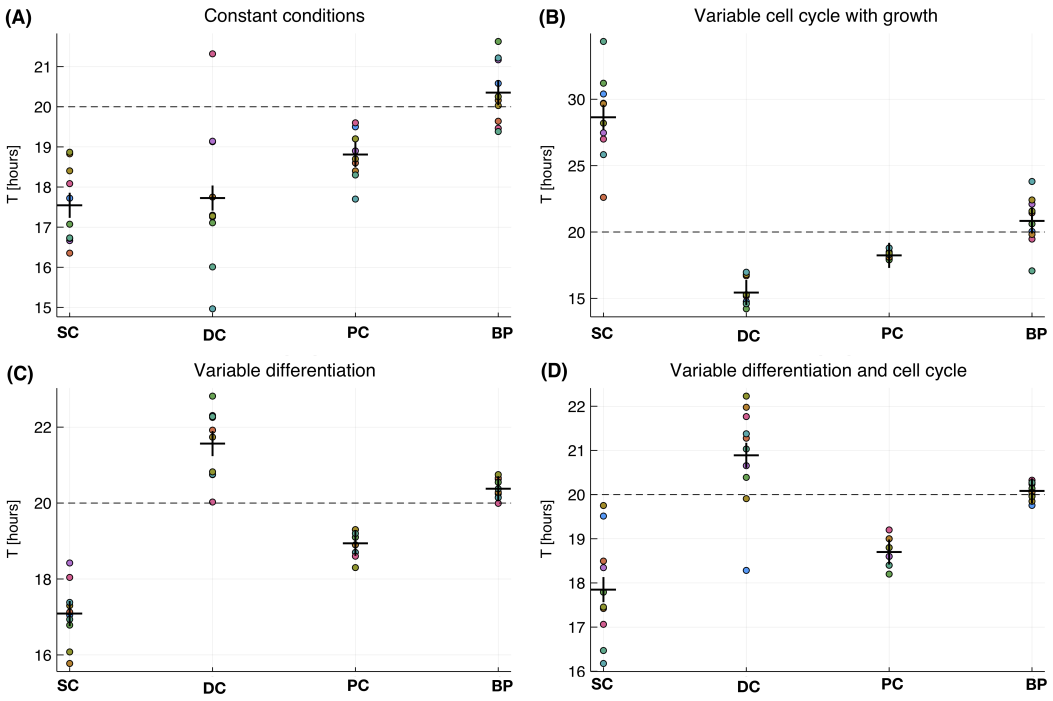

Figure 10: **Supplementary Figure 4: Values of cell cycle predicted for different conditions of growth and differentiation of the culture.** Dots correspond to independent simulations. Crosses represent the average between 10 simulations. Dashed horizontal line corresponds to the average value of T used in the simulations (20 hours). Shorter distance between crosses and dashed line represent better performance of the method. Lower dispersion between dots in each method represents better accuracy. (A) Predicted value of T by each method in conditions of constant mode and rate of division, but for values of increased in the population of progenitors ($pp - dd > 0$). (B) Predicted value of T by each method in conditions where the cell cycle is set to decrease and then increase. (C) Predicted value of T by each method in conditions where the differentiation is increasing monotonically during the simulation. (D) Predicted value of T by each method in conditions where both cell cycle and differentiation rate are set to change during the simulation.

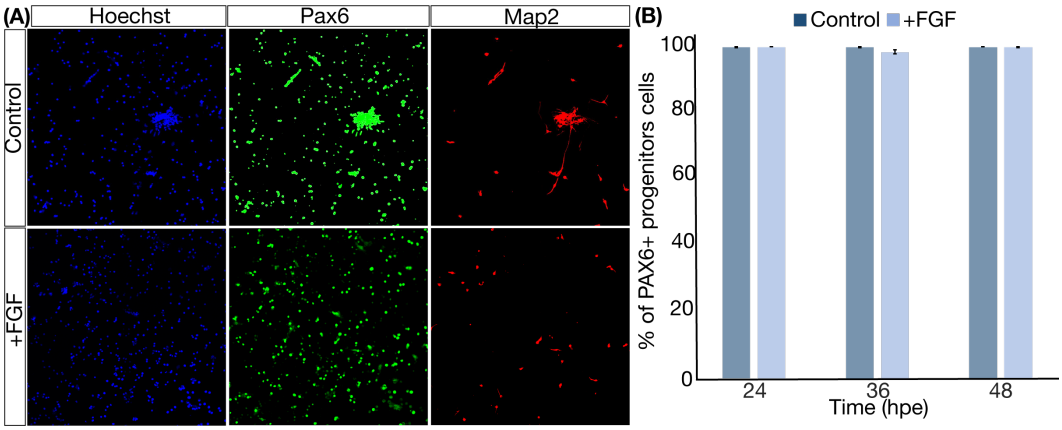

Figure 11: **Supplementary Figure 5. All progenitors cells in the culture express markers of RG.** (A) Example of cells stained with nuclei marker (blue), Pax6 (green), and Map2 (red) at 36 hpe. (B) Quantification of the percentage of progenitors that are Pax6 positive for all conditions and three time points. Columns represent the mean between independent quantifications. Error bars represent the standard error or the mean.